Observations of Wall Slip and Shear Banding in an Entangled DNA Solution

Pouyan E. Boukany

Department of Polymer Science, University of Akron, Akron, Ohio 44325

Y. Thomas Hu*

Unilever Research and Development, 40 Merritt Blvd, Trumbull, Connecticut 06611

Shi-Qing Wang*

Department of Polymer Science, University of Akron, Akron, Ohio 44325

Received October 19, 2007; Revised Manuscript Received January 16, 2008

ABSTRACT: We have studied nonlinear flow behavior of entangled DNA solutions using particle tracking velocimetry in Couette and cone/plate geometries. At apparent shear rate $\dot{\gamma}_{app} < 0.1\ s^{-1}$, the velocity profile is linear across the gap. Beyond the terminal region with $\dot{\gamma}_{app} < 40\ s^{-1}$, the velocity profile becomes temporarily banded after the stress maximum and shows massive wall slip at long times with little shear banding in the bulk. At $\dot{\gamma}_{app} > 40\ s^{-1}$, the velocity profile progressively curves and becomes banded with a sharp interface after hundreds of strain units. In the steady state, the thickness of high-shear band increases linearly with the apparent shear rate. At $\dot{\gamma}_{app} = 1000\ s^{-1}$, the velocity profile returns to linearity.

I. Introduction

A most important task in polymer rheology is the experimental determination and theoretical depiction of nonlinear flow behavior. Previous measurements[1–7] have produced a clearly monotonic relationship between the imposed shear rate and the resulting "steady-state" shear stress, with few exceptions where a slope of stress vs rate was very small.[8–12] Because of this monotonic relationship, it is generally believed that shear flow of entangled polymers should be homogeneous. Guided by this common view, theoretical work has focused on modifying the original Doi–Edwards theory[13] to match the predicted nonlinear flow behavior with the measured monotonic flow curves.

Thus, the recent experimental findings[14] of shear banding in startup shear[15–18] and large-amplitude oscillatory shear (LAOS)[19,20] in entangled polymer solutions came as a surprise. Even more remarkable was the observation of macroscopic motions in the sample interior after a large step strain.[21,22] These results appear to suggest that the entanglement network is rather fragile. It remains an intriguing question whether the shear banding observed in startup shear is merely a transient phenomenon. Previous investigations did not properly answer this question because the shearing experiment was typically aborted after 50 shear strain units to avoid complications such as edge fracture. It is questionable whether a true steady state was reached in these particle-tracking velocimetric (PTV) observations.

It is desirable to examine a model solution that is sufficiently entangled yet free of any inherent experimental difficulties such as edge fracture and rod climbing. Solutions of deoxyribose nucleic acid (DNA)[23] can form entanglement networks that are ideally soft with a plateau modulus G_p in the range of 10−100 Pa. Although single-DNA studies[24–28] have received considerable attention thanks to new tools such as the optical tweezers,[29,30] few focused on exploring the origin of nonlinear rheological behavior of well-entangled DNA solutions. The Stanford group extensively investigated individual dynamics of λ-phage DNA in dilute to entangled systems under various external conditions including uniform (nonshearing) flow,[31,32] elongational flow,[33–37] or steady shear flow[38–44] and during relaxation.[44,45] These pioneering studies revealed crucial information about chain conformational changes and dynamic individualism but did not report any flow inhomogeneity.

In this work, we study a well-entangled DNA solution using two different particle-tracking velocimetric setups and demonstrate without ambiguity that permanent shear banding occurs in the nonlinear flow regime.

II. Experimental Section

A. Materials. The model system is made of a linear double-strand DNA (dsDNA) calf thymus with a weight-average molecular weight of 50×10^6 g/mol or 7.5×10^4 base pairs (bp) (USB Co., used as received). The sample was prepared by dissolving 10 mg/mL of dehydrated DNA in an aqueous buffer containing 10 mM Tris-HCl (pH 7.9), 0.2 mM EDTA, and 10 mM NaCl at room temperature ($T \sim 23$ °C). To inhibit degradation, the DNA solution was stored in refrigerator at $T \sim 4$ °C after mixing. 300 ppm of silver-coated particles (Dantec Dynamic HGS-10) was dispersed in the DNA solution for tracking the velocity profile.

The radius of gyration R_g of our DNA is 1.1 μm according to $R_g = 2l_p(aN/12l_p)^{\nu}$, where $a = 0.34$ nm is the length of base pair, $N = 7.5 \times 10^4$ bp, the persistence length $l_p \sim 0.050$ μm involving 150 bp, and $\nu = 0.5$ for a Θ solvent. The contour length L is 25.5 μm according to $L = aN$. The critical overlap concentration C^*, given by $C^* \sim \rho N/R_g^3$, is 0.062 mg/mL, where $\rho = 1.1 \times 10^{-21}$ g/bp is the linear mass per base pair.[46]

B. Methods. Most velocity profiles were measured in the velocity and velocity gradient plane using a custom-built particle tracking velocimetry (PTV) setup, based on a circular Couette flow cell coupled to a controlled stress rheometer (MCR500, Anton Paar). The flow cell is made of a cup and bob of diameters 35 and 34 mm, respectively (denoted as CO35−34), where there is an inherent stress gradient of 6% across the gap. The conventional rheometric and PTV measurements were made simultaneously. The temperature of the cup was kept at 23 ± 0.1 °C. More details of the Couette PTV setup can be found elsewhere.[47]

Some PTV and rheological experiments were also performed in cone−plate using a second rheometer (Physica MCR-301, Anton

* Corresponding authors. E-mail: thomas.hu@unilever.com or swang@uakron.edu.

10.1021/ma702332n CCC: $40.75
Published on Web 02/29/2008

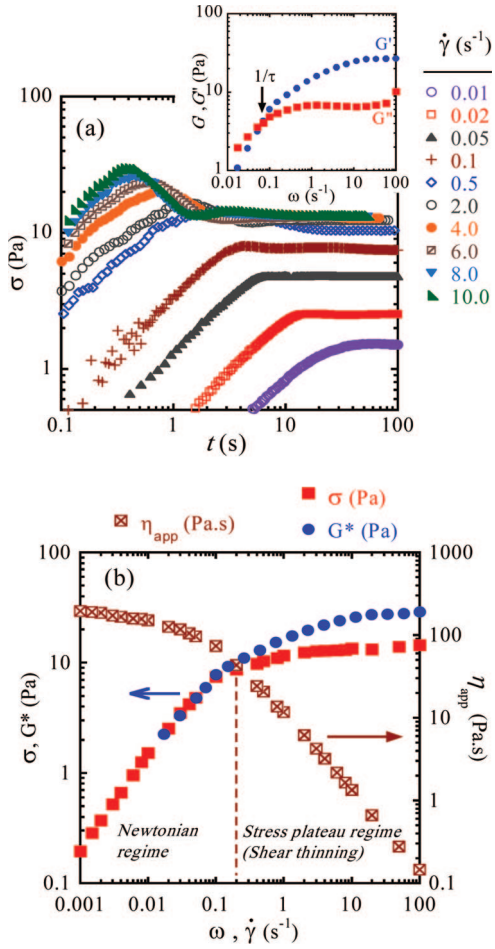

Figure 1. (a) Shear stress growth in startup shear experiment at different imposed shear rates. The inset shows storage and loss moduli (G' and G'') from small-amplitude (5%) oscillatory shear (SAOS) measurements. (b) Flow curve from SAOS and startup shear measurements. Flow geometry: CP25–2. $T = 23$ °C.

Paar) at room temperature ($T \sim 23$ °C). For conventional rheological measurements, a cone of angle 2° and diameter 25 mm (CP25−2) was employed. To prevent water evaporation during rheological measurements, the meniscus of the aqueous DNA solution in the cone−plate cell was surrounded by a low-molecular-weight poly(dimethylsiloxane). The PTV setup consisted of a cone of angle 4° and diameter 25 mm (CP25–4). A flexible transparent film was wrapped around the meniscus. The observation plane was 3–4 mm from the meniscus. A detailed description of the PTV setup has been reported before.[15,16]

III. Experimental Results

A. Linear and Nonlinear Conventional Rheological Measurements. The model solution has a plateau modulus G_p of 27 Pa and terminal relaxation time τ of 14 s as can be read from the inset of Figure 1a. The entanglement molecular weight M_e can be estimated to be 0.91×10^6 g/mol according to $M_e(C) = CRT/G_p(C)$, where C, R, and T are the concentration, gas constant, and temperature, respectively. Hence, there are about $Z = M_w/M_e(C) = 55$ entanglements per chain. Given the value of τ, we can also estimate Rouse relaxation time τ_R as $\tau/3Z \approx 0.08$ s.

The transient behavior including the stress overshoot as shown in Figure 1a is reminiscent of that in other entangled polymer solutions. Taking steady state values of σ and $\eta_{app} = \sigma/\dot{\gamma}_{app}$, we can plot a flow curve as shown in Figure 1b. Although the flow curve appears monotonic, the saturation of shear stress with increasing rate is rather notable.

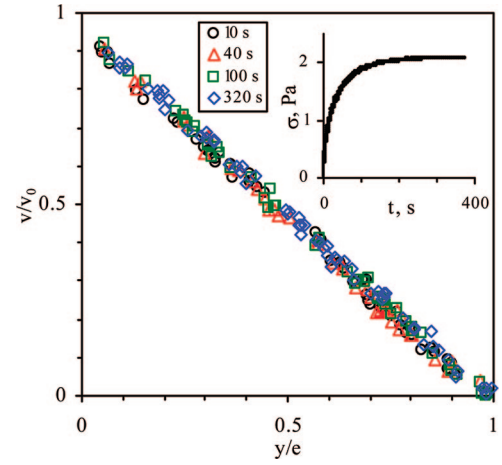

Figure 2. Transient velocity profiles normalized by the imposed inner cylinder surface velocity v_0 at $\dot{\gamma}_{app} = 0.01$ s^{-1}. y is the radial distance to the inner surface, and e is the gap width. ($y/e = 0$ and 1 correspond to the rotational inner and stationary outer cylinder surfaces, respectively.) Upper right corner inset shows the stress response. Flow geometry: CO35–34. $T = 23$ °C.

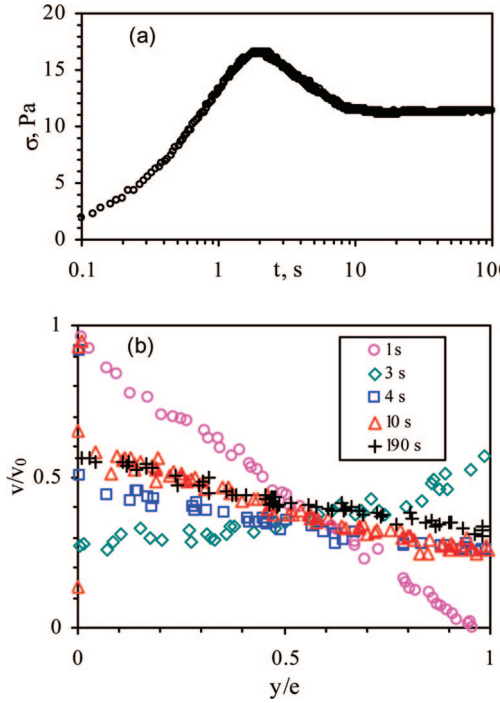

Figure 3. Transient behavior at $\dot{\gamma}_{app} = 1.0$ s^{-1}: (a) shear stress; (b) velocity profiles at various times. At $t = 3$ s, the velocity profile has a positive slope, indicating negative local shear rates. Flow geometry: CO35–34. $T = 23$ °C.

B. PTV Measurements: Time Dependence. *1. Homogeneous Shear in Linear (Terminal) Regime ($\dot{\gamma}_{app} < \tau^{-1}$).* At low imposed apparent shear rates $\dot{\gamma}_{app} \leq 0.1$ s^{-1}, the velocity profile is approximately linear during shearing at all times as shown in Figure 2. The agreement between the prescribed shear rate and the PTV measured value indicates there is little wall slip in this terminal regime.

2. Wall Slip and Fluctuation of Velocity Profile at Intermediate Shear Rates $\dot{\gamma}_{app} \leq 40$ s^{-1}. Couette Flow Cell: At $\dot{\gamma}_{app} \leq 0.1$ s^{-1}, a stress overshoot occurs at $\gamma \approx 2$ (Figure 3a). Before the overshoot, $t \leq 2$ s, the velocity increases linearly toward the rotating inner wall. At $t = 3$ s, the velocity profile changes dramatically, showing recoil-like behavior and strong wall slip (Figure 3b). This behavior appears during the stress decline after

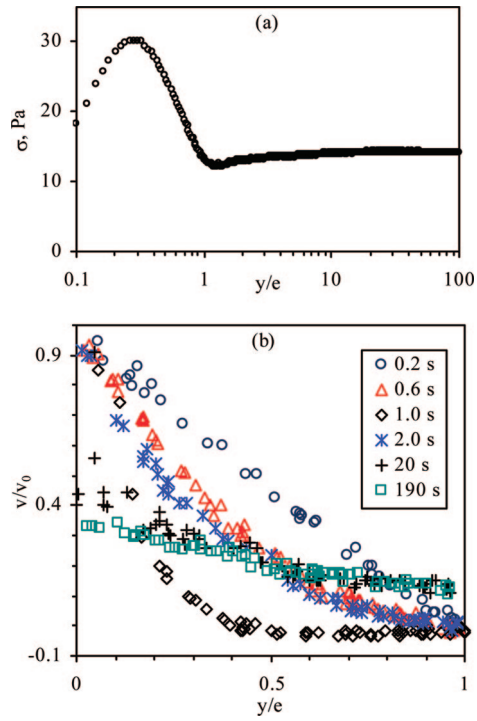

Figure 4. Transient behavior at $\dot{\gamma}_{app} = 10.0\ s^{-1}$: (a) shear stress; (b) velocity profiles. At $t = 1$ s, the velocity profile is "banded", and the slope of outer portion ($y/e > 0.5$) is slightly positive, indicating negative local shear rates. Flow geometry: CO35–34. $T = 23$ °C.

the primary stress maximum on the stress curve in Figure 3a. At and beyond $t = 4$ s, wall slip becomes more or less stable at both inner and outer walls. At long times, the velocity profile keeps making small adjustment, with an average shear rate of about 0.3 s^{-1} in the bulk. At $\dot{\gamma}_{app} = 10\ s^{-1}$, the velocity profile is also linear before the stress overshoot, which now shifts to a larger strain of 3, as shown in Figure 4. At $t = 1$ s, strong wall slip occurs and the velocity profile becomes briefly banded. At $t = 2$ s, the velocity profile becomes smoothly curved and wall slip disappears. At longer times, wall slip occurs again and the velocity profile becomes less curved. Similar transient behavior was observed for $\dot{\gamma}_{app}$ up to 40 s^{-1}. At $\dot{\gamma}_{app} > 40\ s^{-1}$, the imposed shear is too fast for the PTV technique (with the time resolution of 0.2 s) to capture the transient velocity profiles before the stress minimum.

Cone−Plate Shear Cell: The transient behavior in cone−plate (Figure 5a,b) is similar to that in the Couette cell.[48] The velocity profile is linear up to the shear stress peak but becomes nonlinear after the stress overshoot. The velocity profile is unstable and fluctuates with strong wall slip even at long times. This PTV setup for cone−plate cell is limited to $\dot{\gamma}_{app} < 10\ s^{-1}$.

3. Permanent Shear Banding at High Shear Rates $\dot{\gamma}_{app} > 40\ s^{-1}$. Figure 6a shows typical transient behavior in the Couette cell. The velocity profile evolves in four different stages, corresponding to the various stages of the transient shear stress:

Stage I (before the first stress maximum, not captured at $\dot{\gamma}_{app} = 150\ s^{-1}$): The velocity profile is presumably linear as observed at lower shear rates and previous publications.[15–17]

Stage II (between the first stress maximum and minimum, $t < 0.4$ s): Figure 6b shows that the velocity profile becomes significantly bent ($t = 0.2$ s) first and subsequently less curved ($t = 0.4$ s) as the stress decreases rapidly. The corresponding shear rate profile indicates in Figure 6c that the local shear rate is strongly inhomogeneous across the gap at $t = 0.2$ s, with the high shear regime located at the inner side, becoming less inhomogeneous at $t = 0.4$ s.

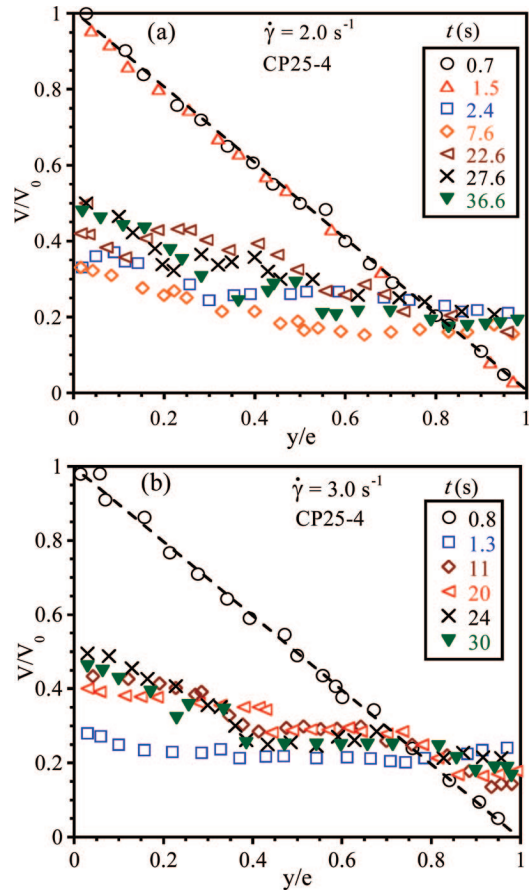

Figure 5. Time evolution of velocity profile in cone−plate shear at (a) $\dot{\gamma}_{app} = 2.0\ s^{-1}$ and (b) $\dot{\gamma}_{app} = 3.0\ s^{-1}$. Here *X*-axis positions $y/e = 0$ and 1 correspond to the rotational and stationary surfaces, respectively. *Y* axis $V/V_0 = 0$ and 1 correspond to normalized velocity of stationary and rotational surfaces. Flow geometry CP25–4. $T = 23$ °C.

Stage III (between the primary stress minimum and second maximum, $0.4 < t < 5$ s): The velocity profile becomes increasingly curved but remains smooth. The shear rate keeps increasing near the inner side and decreasing the rest of the region. The shear rate remains continuous across the gap.

Stage IV (second stress maximum to plateau, $t > 5$ s, inset of Figure 6a): The velocity profile becomes extremely curved, and two distinct flow regimes are apparent with a sharp interface. The local shear rate becomes discontinuous, and a high and low shear bands can be discerned. Over time, the shear rate in the high shear band further increases and that in the low shear band decreases. The low shear band expands toward the inner side until the steady state is reached at $t \approx 10$ s for both the stress and the velocity profile. Similar transient behavior is observed at other high shear rates.

4. Disappearance of Shear Banding. At an applied shear rate $\dot{\gamma}_{app} = 1000\ s^{-1}$, the velocity profile is approximately linear as shown in Figure 7. There is no significant curving or banding at any stage beyond 0.2 s. The local shear rate $\dot{\gamma}(y)$ decreases from 1142 s^{-1} at the inner wall to 823 s^{-1} at the outer wall, with an average value of 971 s^{-1}. The 38% of spatial variation in the shear rate across the gap is much larger than the inherent stress gradient of 6% of the geometry, indicating shear thinning behavior with a power law index of $n = 0.18$ for $\sigma \sim \dot{\gamma}^n$. No significant viscous heating or rod climbing was observed even at this high shear rate.

5. Shear Band Relaxation and Re-formation. In a relaxation test shown in Figure 8, the sample was first sheared at $\dot{\gamma}_{app} = 300\ s^{-1}$ for 20 s to allow shear bands to fully develop. The applied rate was then stepped down abruptly (within mil-

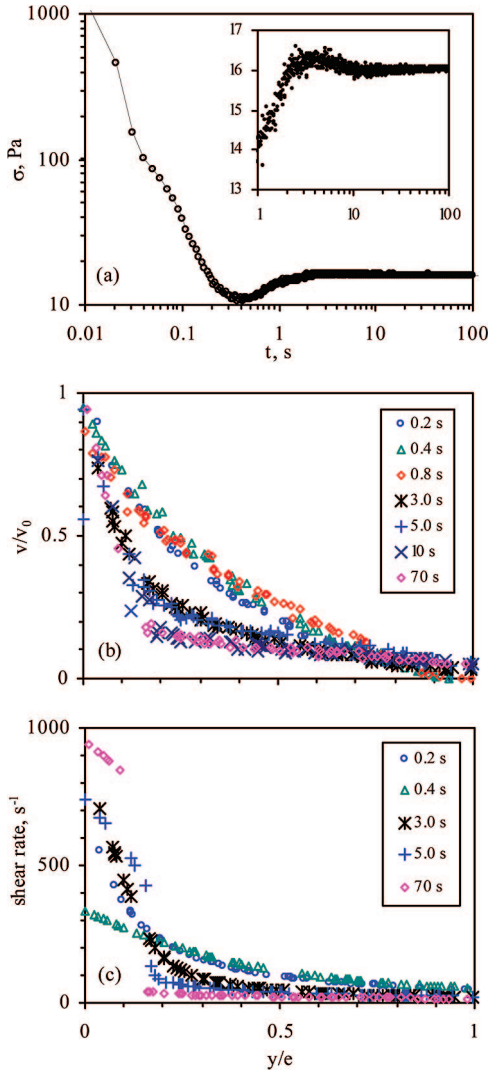

Figure 6. Transient behavior in step shear with $\dot{\gamma}_{app} = 150\ s^{-1}$: (a) shear stress. The inset is a blowout of the same data showing the second stress maximum; (b) velocity profiles; (c) shear rate profiles. Flow geometry: CO35–34. $T = 23$ °C.

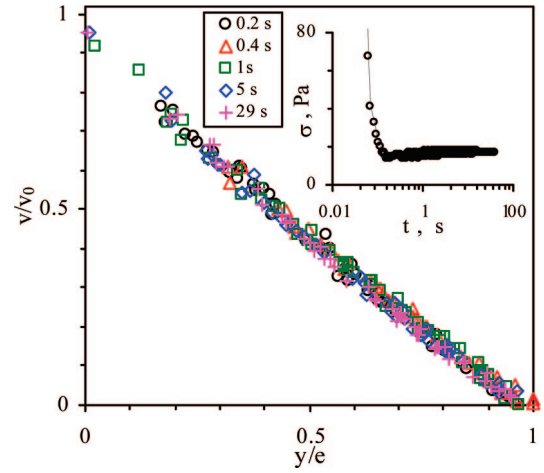

Figure 7. Transient velocity profiles in step shear with $\dot{\gamma}_{app} = 1000\ s^{-1}$. Upper right corner inset: shear stress response. Flow geometry: CO35–34. $T = 23$ °C.

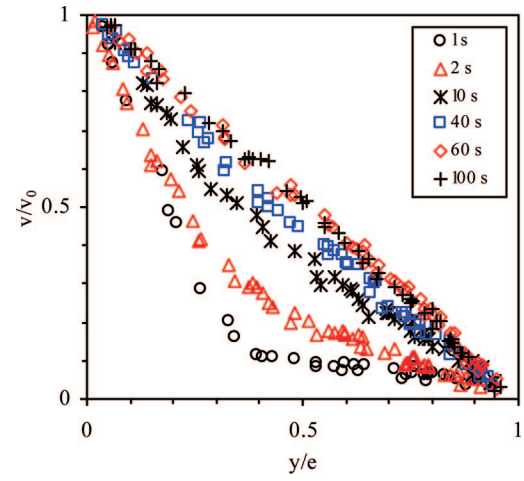

Figure 8. Time evolution of the velocity profile after the shear rate is stepped down from $\dot{\gamma}_{app} = 300$ to $0.1\ s^{-1}$. Linear velocity profile is recovered in about 60 s. Flow geometry: CO35–34. $T = 23$ °C.

liseconds time scale) to $\dot{\gamma}_{app} = 0.1\ s^{-1}$, and the change of the velocity profile was monitored in order to probe the lifetime of the inhomogeneity. The velocity profile remains banded briefly for 1 s after the shear rate step-down and then becomes smoothly curved. It takes at least 40 s for the velocity profile to become linear, which signifies return of a homogeneous state.

Figure 9 shows another set of experiments designed to probe the lifetime of the shear bands. The sample was first sheared from a well-rested state for 20 s to allow shear bands to fully develop. The flow was then completely turned off for a range of resting times to allow the shear bands to relax, after which it was turned on again. The re-formation of shear bands following a resting time of 200 s repeats the first in its original full time evolution. In contrast, development of the shear banding is much faster than the original when the resting time is only 50 s (Figure 10). These experiments indicate that the effective lifetime of shear bands is between 50 and 200 s. (Note that these tests were performed after the sample had sit in the flow cell overnight. It is likely that the DNA concentration had changed somewhat, which might be responsible for the different interface position from that in Figure 11b at $300\ s^{-1}$.)

C. PTV Measurements: Steady State. The steady-state velocity profiles at various applied average shear rate ranging from 0.01 to $1000\ s^{-1}$ are summarized in Figure 11a. The local shear rate in either the low or high shear regime is not constant but increases with $\dot{\gamma}_{app}$, as shown in Figure 11b. The width of the high shear regime increases approximately linearly with $\dot{\gamma}_{app}$. The velocity profile indicates that the apparent shear rate is generally not the true shear rate. Thus, the directly measured stress vs apparent shear rate flow curve given in Figure 1b does not represent a true constitutive relation of the system.

IV. Discussion

A. Nature of Wall Slip. Violation of no-slip boundary conditions has been extensively studied[49] for entangled polymer melts[50] and solutions.[51] At intermediate shear rates $0.5 < \dot{\gamma}_{app} < 10\ s^{-1}$, the sliplike behavior is dominant during startup shear after the stress overshoot in both cone−plate and Couette cells. True wall slip, i.e., lack of interfacial entanglement, can indeed be appreciable since the solvent viscosity of water is exceedingly lower relative to the solution viscosity. According to the following formula for the Navier−de Gennes extrapolation length b, we can estimate the magnitude of wall slip

$$b = (\eta / \eta_i) a_L \tag{1}$$

where the ratio of the bulk to interfacial viscosity (η/η_i) is very large, and the entanglement spacing a_L typically defines the interfacial layer thickness. According to $a_L^2 = 6R_g^2/Z(C)$ and

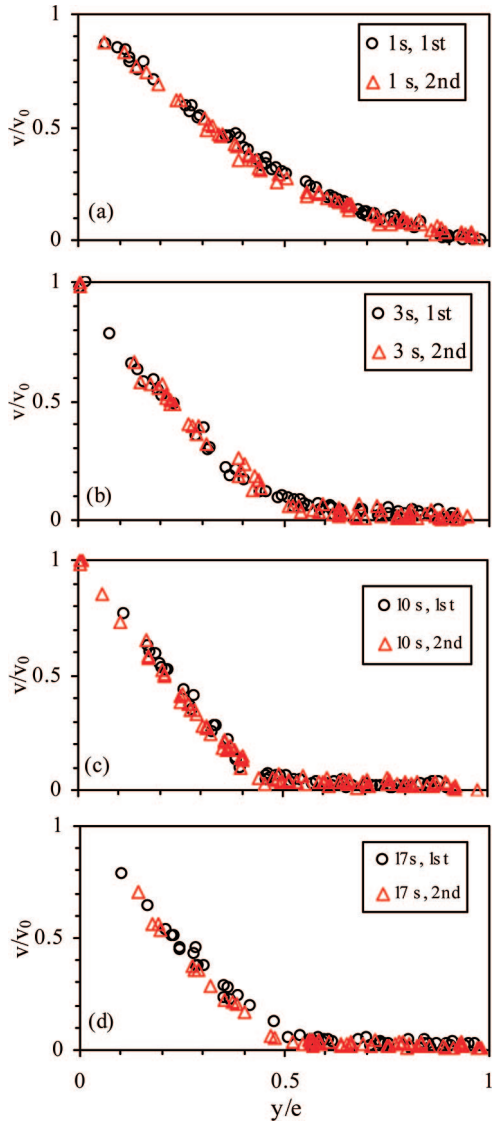

Figure 9. Comparison of time evolution of the velocity profile between back-to-back tests. First run: shear banding process from a well-rested state. Second run: time sequence of re-formation of shear bands after the previous fully developed shear bands have relaxed for 200 s. Time in the figure indicates shear time for each run at $\dot{\gamma}_{app} = 300\ s^{-1}$. Flow geometry: CO35–34. $T = 23$ °C.

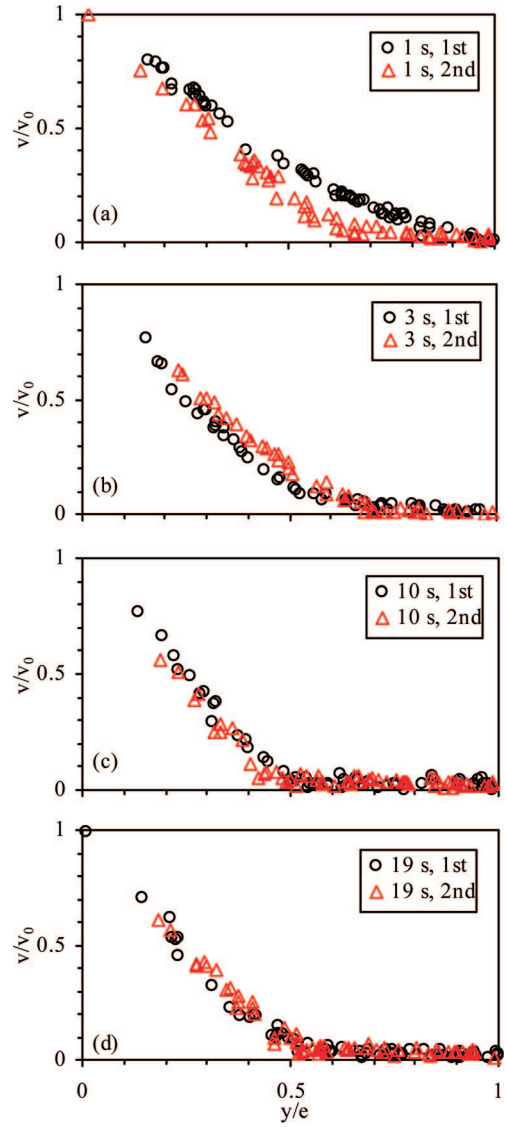

Figure 10. Comparison of time evolution of the velocity profile between back-to-back tests. First run: shear banding process from a well-rested state. Second run: time sequence of re-formation of shear bands after the previous fully developed shear bands have relaxed for 50 s. Time on figure indicates shear time for each run at $\dot{\gamma}_{app} = 300\ s^{-1}$. Flow geometry: CO35–34. $T = 23$ °C.

taking η_i to be 10^{-3} Pa•s of water, we have, by reading η from the Figure 1b to be ca. 190 Pa•s, $b = 6.8$ cm. This estimate indicates that in this aqueous DNA solution interfacial slip in the two flow geometries can greatly alter the flow field and make it pluglike because the characteristic dimension (i.e., the gap distance) is ca. 0.1 cm. Since the borderline between terminal and plateau regions is around $\dot{\gamma}_b \sim 0.2\ s^{-1}$, we can estimate or predict when shear banding other than interfacial slip may emerge with increasing $\dot{\gamma}_{app} = V/H$. At low values of V/H in the stress plateau, $V = \dot{\gamma}_{app}H + 2V_s$, so that $\dot{\gamma}_{app}/\dot{\gamma}_b = 1 + 2b/H$, where $b = V_s/\dot{\gamma}_b$. This means that the imposed rate $\dot{\gamma}_{app}$ could increase from $\dot{\gamma}_b \sim 0.2\ s^{-1}$ until $\dot{\gamma}_{app} \sim \dot{\gamma}_b(2b/H) = 27\ s^{-1}$ without developing any shear banding in the bulk, where $H = 1$ mm. For $\dot{\gamma}_{app} > \dot{\gamma}_b(2b/H)$, shear banding may become observable. This analysis is consistent with our PTV observations presented in Figures 3−6 that shear banding emerges at $\dot{\gamma}_{app} > 40\ s^{-1}$.

B. Transient Inhomogeneous Shear after Stress Overshoot. After the stress overshoot, the velocity profile briefly becomes severe nonlinear (Figure 6b). The severe nonlinearity occurs between the primary stress maximum and minimum. Similar transient behavior has been observed in both micellar[47] and polymer systems.[15–17] Chain overorientation and intrinsic stress gradient of the geometry were previously suggested as the cause for temporary strong banding.[17] Cohesive breakup through chain disentanglement was recently proposed to attribute the inhomogeneous shear to structural failure.[52]

C. Permanent Shear Banding. Bulk shear banding are observed at high shear rates in a range of $80 < \dot{\gamma}_{app} < 800\ s^{-1}$. In the following we discuss various factors to explore the origin of the observed shear banding.

Flow-Induced Demixing (Chain Migration). As a wild speculation, suppose the observed shear bands (cf. Figure 6) would reflect presence of two layers of different concentrations due to DNA migration after a long period of shear. We could estimate the time required to homogenize the sheared sample after stopping the flow. Since the DNA molecules re-entangle rapidly upon shear cessation, it is reasonable to estimate t_h according to $t_h/\tau \sim (\Delta x/R_g)^2$ with $\tau = 14$ s being the terminal relaxation time, and $R_g = 1.1\ \mu$m, i.e., $t_h \sim 10^5$ s for $\Delta x = 0.1$

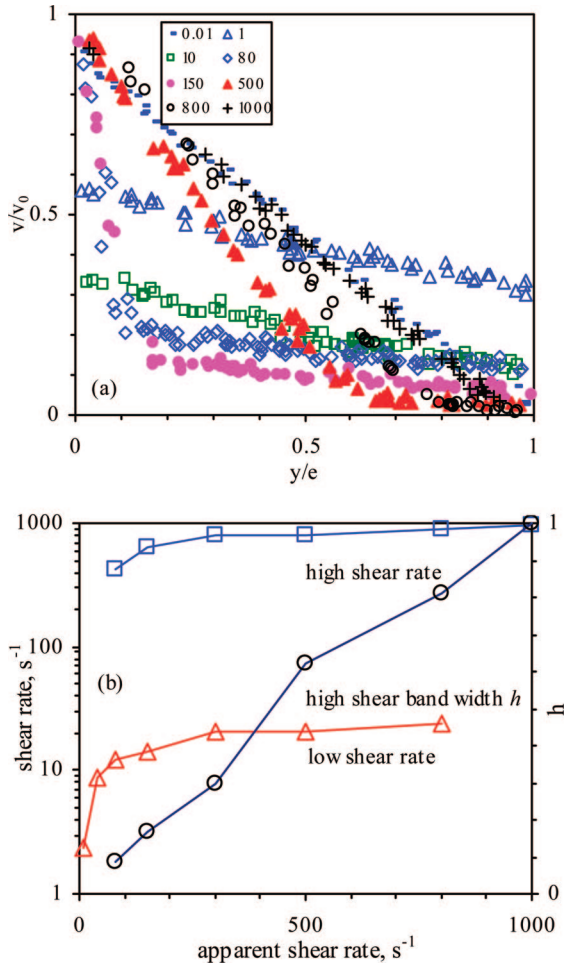

Figure 11. (a) Snapshots of velocity profiles across the flow cell gap in the steady state at various apparent shear rates $\dot{\gamma}_{app}$. (b) Shear rates in the low and high shear bands and the interface position (width of the high shear band). Flow geometry: CO35–34. $T = 23$ °C.

mm, which is longer than 24 h. On the other hand, we know from Figure 9 it takes less than 200 s to completely recover the original homogeneous state after shear banding. Our estimate is based on the perception that mass transport leading to homogenization takes place between two layers of different concentration and thickness on the order of 0.1−1 mm. The chains would have to diffuse from one entanglement network to another by fighting against the entanglement effect. One reviewer commented that the diffusion constant should be the cooperative diffusivity given in de Gennes *Scaling Concepts* book as VII.24. We will await an experimental estimate in the future.

Flow-Induced Chain Scission. It can be asserted that the stress level involved in the present study is several orders of magnitude lower than required to produce chain scission in the DNA molecules. We have verified such an estimate by running small-amplitude oscillatory shear (SAOS) measurements before and after high shear. We found negligible change in the storage and loss moduli G' and G''. Figure 9 also reassures that a presheared sample follows the same banding path to its final velocity profile as the fresh sample. This full reproducibility of shear banding after preshear suggests that there is no shear-induced chain scission.

Edge Instability. Edge instability or free surface distortion in rotational cone-plate or parallel-plate flow cells is a major challenge and concern in the exploration of nonlinear flow behavior of entangled systems. If severe edge instability occurs during measurement, some amount of sample may roll out from the shear cell. For our soft aqueous DNA solution with a plateau modulus under 30 Pa, edge instability is unimportant, due to an exceedingly low level of elasticity. Negligible changes in G' and G'' before and after startup shear were found, suggesting that edge instability or sample loss is negligible. Additionally, permanent shear banding is observed in a Couette flow cell without any evidence of rod climbing and distortion of free surface. The observed shear banding does not appear to originate from edge fracture. Thus, it seems that the observed shear banding reflects true structural change in the bulk. The disappearance of the shear banding at $\dot{\gamma}_{app} = 1000\ s^{-1}$ suggests that the system has exited the stress plateau region in the flow curve, and the DNA chain structures become largely homogeneous again.

We have presented experimental evidence for steady-state shear banding in entangled DNA solutions. In the terminal region with $\dot{\gamma}_{app} < 0.1\ s^{-1}$, the velocity profile is linear across the gap. In the intermediate stress plateau region with $1/\tau < \dot{\gamma}_{app} < 40\ s^{-1}$, the velocity profile is linear up to the stress maximum but becomes temporarily nonlinear, followed by massive wall slip, with little discernible banding in the bulk. For $\dot{\gamma}_{app} > 40\ s^{-1}$, permanent shear banding occurs in steady state. The thickness of high-shear band increases linearly with the apparent shear rate up to $\dot{\gamma}_{app} = 1000\ s^{-1}$, where the velocity profile returns to linearity.

Acknowledgment. This work is supported, in part, by a small grant for exploratory research from National Science Foundation (DMR-0603951) and by a PRF grant from American Chemical Society (#40596-AC7). Y.T.H. is grateful to Alex Lips for encouragement and to Unilever management for permission to publish this work.

References and Notes

(1) Statton, R. A. *J. Colloid Interface Sci.* **1966**, *22*, 517.
(2) Huppler, J. D. *Trans. Soc. Rheol.* **1967**, *11*, 181.
(3) Lee, C. L.; Polmanteer, K. E.; King, E. G. *J. Polym. Sci., Part A-2* **1970**, *8*, 1909.
(4) Graessley, W. W. *Adv. Polym. Sci.* **1974**, *16*, 1.
(5) Crawley, R. L.; Graessley, W. W. *Trans. Soc. Rheol.* **1977**, *21*, 19.
(6) Wagner, M. H.; Meissner, J. *Macromol. Chem.* **1980**, *181*, 1533.
(7) Menezes, E. V.; Graessley, W. W. *J. Polym. Sci., Polym. Phys. Ed.* **1982**, *20*, 1817.
(8) Bercea, M.; Peiti, C.; Simionescu, B.; Navard, P. *Macromolecules* **1993**, *26*, 7095.
(9) Jary, D.; Sikorav, J. L.; Lairez, D. *Europhys. Lett.* **1999**, *46*, 251.
(10) Pattamaprom, C.; Larson, R. G. *Macromolecules* **2001**, *34*, 5229.
(11) Islam, M. T.; Archer, L. A. *J. Polym. Sci., Part B: Polym. Phys.* **2001**, *39*, 2275.
(12) It is challenging to achieve steady state in conventional cone−plate setup for entangled polymer solutions. To avoid edge fracture and accumulating sample rolling over, it is routine to truncate a startup shear experiment after 30 shear strain units, which could be premature and result in inaccurate determination of the steady-state flow curve. See ref 18 for a resolution of this inherent rheometric challenge.
(13) Doi, M.; Edwards, S. F. *The Theory of Polymer Dynamics*, 2nd ed.; Clarendon Press: Oxford, 1988.
(14) Wang, S. Q. *Macromol. Mater. Eng.* **2007**, *292*, 15.
(15) Tapadia, P.; Wang, S. Q. *Phys. Rev. Lett.* **2006**, *96*, 016001.
(16) Boukany, P. E.; Wang, S. Q. *J. Rheol.* **2007**, *51*, 217.
(17) Hu, Y. T.; Wilen, L.; Phlips, A.; Lips, A. *J. Rheol.* **2007**, *51*, 275.
(18) Ravindranath, S.; Wang, S. Q. *J. Rheol.* **2007**, available under Publications at http://www3.uakron.edu/rheology/.
(19) Tapadia, P.; Ravindranath, S.; Wang, S. Q. *Phys. Rev. Lett.* **2006**, *96*, 196001.
(20) Ravindranath, S.; Wang, S. Q. *J. Rheol.* **2008**, in press, available under Publications at http://www3.uakron.edu/rheology/.
(21) Wang, S. Q.; Ravindranath, S.; Boukany, P.; Olechnowicz, M.; Quirk, R.; Halasa, A.; Mays, J. *Phys. Rev. Lett.* **2006**, *97*, 187801.
(22) Ravindranath, S.; Wang, S. Q. *Macromolecules* **2007**, *40*, 8031.
(23) Laib, S.; Robertson, R. M.; Smith, D. E. *Macromolecules* **2006**, *39*, 4115.
(24) Smith, S. B.; Finzi, L.; Bustamante, C. *Science* **1992**, *258*, 1122.
(25) Bustamante, C.; Marko, J. F.; Siggia, E. D.; Smith, S. *Science* **1994**, *265*, 1599.

(26) Bao, G. *J. Mech. Phys. Solids* **2002**, *50*, 2237.
(27) For a review see: Peyrard, M. *Nonlinearity* **2004**, *17*, R1.
(28) Shaqfeh, E. S. G. *J. Non-Newtonian Fluid Mech.* **2005**, *130*, 1 and references therein.
(29) Perkins, T. T.; Smith, D. E.; Chu, S. *Science* **1994**, *264*, 819.
(30) Quaker, S. R.; Babcock, H. P.; Chu, S. *Nature (London)* **1997**, *388*, 151.
(31) Perkins, T. T.; Smith, D. E.; Larson, R. G.; Chu, S. *Science* **1995**, *268*, 83.
(32) Smith, D. E.; Perkins, T. T.; Chu, S. *Macromolecules* **1996**, *29*, 1372.
(33) Perkins, T. T.; Smith, D. E.; Chu, S. *Science* **1997**, *276*, 2016.
(34) Smith, D. E.; Chu, S. *Science* **1998**, *281*, 1335.
(35) Babcock, H. P.; Teixeria, R. E.; Hur, J. S.; Shaqfeh, E. S. G.; Chu, S. *Macromolecules* **2003**, *36*, 4544.
(36) Schroeder, C. M.; Babcock, H. P.; Shaqfeh, E. S. G.; Chu, S. *Science* **2003**, *301*, 1515.
(37) Schroeder, C. M.; Shaqfeh, E. S. G.; Chu, S. *Macromolecules* **2004**, *37*, 9242.
(38) Smith, D. E.; Babcock, H. P.; Chu, S. *Science* **1999**, *283*, 1724.
(39) Babcock, H. P.; Smith, D. E.; Hur, J. S.; Shaqfeh, E. S. G.; Chu, S. *Phys. Rev. Lett.* **2000**, *85*, 2018.
(40) Hur, J. S.; Shaqfeh, E. S. G.; Babcock, H. P.; Smith, D. E.; Chu, S. *J. Rheol.* **2001**, *45*, 421.
(41) Teixeria, R. E.; Babcock, H. P.; Shaqfeh, E. S. G.; Chu, S. *Macromolecules* **2005**, *38*, 581.
(42) Schroeder, C. M.; Teixeria, R. E.; Shaqfeh, E. S. G.; Chu, S. *Macromolecules* **2005**, *38*, 1967.
(43) Schroeder, C. M.; Teixeria, R. E.; Shaqfeh, E. S. G.; Chu, S. *Phys. Rev. Lett.* **2005**, *95*, 018301.
(44) Teixeria, R. E.; Dambal, A. K.; Richter, D. H.; Shaqfeh, E. S. G.; Chu, S. *Macromolecules* **2007**, *40*, 2461.
(45) Perkins, T. T.; Quaker, S. R.; Smith, D. E.; Chu, S. *Science* **1994**, *264*, 822.
(46) Mason, T. G.; Dhople, A.; Wirtz, D. *Macromolecules* **1998**, *31*, 3600.
(47) Hu, Y. T.; Lips, A. *J. Rheol.* **2005**, *49*, 1001.
(48) More results based on cone−plate PTV setup than given in this paper were first presented at the 78th Society of Rheology Annual Meeting on October 12, 2006, titled "Disentanglement behavior of DNA solutions as probed with particle-tracking velocimetry".
(49) Wang, S. Q. *Adv. Polym. Sci.* **1999**, *138*, 227.
(50) Boukany, P. E.; Wang, S. Q. *J. Rheol.* **2006**, *50*, 641.
(51) Plucktaveesak, N.; Wang, S. Q. *Macromolecules* **1999**, *32*, 3045.
(52) Wang, S. Q.; Ravindranath, S.; Wang, Y.; Boukany, P. *J. Chem. Phys.* **2007**, *127*, 064903.

MA702332N